Low-Complexity High-Resolution Parameter Estimation for Automotive MIMO Radars

YU-CHIEN LIN[ID], TA-SUNG LEE[ID], (Fellow, IEEE), YUN-HAN PAN, AND KUAN-HEN LIN

Center for mmWave Intelligent Radar Systems and Technologies, Institute of Communications Engineering, National Chiao Tung University, Hsinchu 30010, Taiwan

Corresponding author: Ta-Sung Lee (tslee@mail.nctu.edu.tw)

ABSTRACT In this paper, we propose a parameter estimation method for multiple-input-multiple-output (MIMO) automotive radars that consists of two stages. The first stage is a low-complexity three-dimensional (3D) constant false alarm rate (CFAR) detection technique that exploits spatial filtering to extend radar coverage, and it performs low-complexity peak detection. The second stage is an ESPRIT-based direction-of-arrival (DOA) estimation technique that adopts time–frequency resource division to generate high-quality snapshots and it performs DOA estimation of targets without the knowledge of the target number. Computer simulations reveal that the proposed method achieves the performance of the two-dimensional ordered statistic CFAR (2D OS-CFAR) while having much lower computational complexity, and it offers the higher resolution DOA estimation compared to the conventional MIMO radars.

INDEX TERMS MIMO radar, mmWave radar, CFAR detection, DOA estimation, ESPRIT.

I. INTRODUCTION

With the increasing number of vehicles, the probability of road traffic accidents has consequently increased. In actual driving situations, a vehicle safety system can provide early warning for accidents by reminding drivers or actively controlling vehicles to prevent dangerous situations and thus protect the driver [1]. To provide the required safety functionality, the system must grasp accurate real-time traffic information of surrounding vehicles. Most vehicle safety systems employ radar as a primary sensor for target detection. Thus, to achieve the above safety objective, signal processing methods for automotive radars having high performance and robustness and low complexity must be designed.

Frequency modulated continuous wave (FMCW) and orthogonal frequency division multiplexing (OFDM) waveforms in automotive radars are widely discussed. They can provide high-resolution measurements of the target's range and velocity [2]. Compared to other radar systems, including pulse radar, they have low measurement time and peak-to-average power ratio [3]. FMCW and OFDM radars obtain

range and velocity information from the sinusoidal components, which directly reflect the target's propagation delay and Doppler shift [4]. To detect the sinusoidal components of targets in the spectrum, a peak detector is required. When considering noise, the constant false alarm rate (CFAR) detector is widely preferred for peak detection in radar systems [5].

CFAR detectors evaluate the average power level of noise according to cells neighboring the cell under test (CUT) and set an appropriate detection threshold. Conventional CFAR detectors include cell-average CFAR (CA-CFAR) and order-statistic CFAR (OS-CFAR). CA-CFAR averages the power of neighboring cells to evaluate the noise power. However, neighbor cells may not represent the noise in multi-target scenarios [6]. Thus, CA-CFAR often overestimates the average noise and degrades the detection probability. In contrast, OS-CFAR determines the threshold based on the relative magnitude of neighboring cells. The selected order and corresponding threshold can be determined using the OS-CFAR detector, which is more robust than CA-CFAR in multi-target scenarios [7].

The above-mentioned CFAR detectors and some modified CFAR detectors with binary integration [8] are adopted to handle most scenarios, but they still have drawbacks,

including loss of detection of objects with a small radar cross section or objects located at the boundary of the field-of-view (FOV) of radars with a small antenna gain, and high computational complexity in noise-level estimation.

However, to obtain reliable target information, accuracy, and resolution in range, the Doppler velocity and direction-of-arrival (DOA) of targets are required. Although these requirements can be fulfilled by exploiting more resources in the time and frequency domains and increasing computational complexity, DOA estimation is restricted by the number of antennas on the radar.

DOA estimation techniques can be divided into beamforming, subspace and parametric types [9]. The conventional beamforming technique steers the beam towards different directions and determine the target DOA at the peak beam response. It has poor resolution for close targets. MVDR [10], [11], RELAX [12] and FIIB [13] are improved beamforming techniques having higher resolution but also higher complexity. The subspace techniques exploit the Eigen-structure of the spatial signal correlation matrix, two popular examples being MUSIC [14] and ESPRIT [15]. The parametric techniques exploit the spatial signal model directly, with maximum likelihood (ML) [16] and subspace fitting (SF) [17] being two well-known estimators. Both the subspace and parametric techniques can achieve significantly higher resolution than the conventional beamforming technique while requiring higher complexity. In general, the subspace techniques offer the best compromise between resolution and complexity among the three types of technique.

Two major concerns exist in subspace-based DOA estimation techniques. First, they could degrade owing to coherent signals. In automotive radars, returns are coherent because they originate from the same source. Spatial smoothing is an effective means of decorrelating coherent signals for uniform linear array (ULA) [18]–[20]. In [21], an ESPRIT-like technique can decorrelate coherent signals at the cost of a 50% reduction in array aperture. Second, they usually require *a priori* information of the target number. Although reliable target number detectors [22], [23] are available, they also degrade for coherent signals. New techniques have been proposed that do not require knowledge of target number. In [24], an improved version of [21] works with a spatial spectrum function independent of target number. In [25], a MUSIC-like technique is realized in the framework of beamforming and does not require target number information.

We propose a parameter estimation method for multiple-input-multiple-output (MIMO) automotive radars to address these issues. The method comprises a low-complexity beamforming-aided CFAR detection technique and an ESPRIT-based DOA estimation technique. ESPRIT is adopted because it allows a flexible array geometry and makes a simple criterion for target number determination feasible, as described in Section IV.C. For the proposed CFAR detection technique, we first exploit spatial filtering

to enhance the SNR of target returns. Computational cost is then reduced by a transformation from 3D CFAR detection to two 1D CFAR detections. For the proposed DOA estimation technique, we first exploit time-frequency (T-F) division to generate sufficient snapshots for DOA estimation. Spatial and frequency decorrelation is then employed to decorrelate coherent target returns. Finally, ESPRIT is employed to perform DOA estimation aided by a proposed criterion for discriminating closely spaced targets.

The remainder of the paper is organized as follows. Section II presents the system model. Section III describes the low-complexity 3D CFAR detection. Section IV details the ESPRIT-based DOA estimation technique. Section V gives the simulation results. Finally, Section VI draws the conclusions.

II. SYSTEM MODEL

We here consider a scenario where one monostatic multiple-input-multiple-output (MIMO) radar is equipped on a vehicle. The desired target parameters are the range, relative Doppler velocity, and DOA of each target to observer. Although the proposed method in this paper can be applied to both FMCW and OFDM radars, OFDM radar offers the advantage of flexibility of T-F resource allocation. Without loss of generality, the paper will concentrate on a single monostatic OFDM radar for which the interference from other vehicles' radars can be treated as additive white Gaussian noise (AWGN) [26].

A. OFDM RADAR SIGNAL MODEL

OFDM is a method of encoding digital data at orthogonal subcarriers. In this paper, an OFDM symbol is composed of N subcarriers, each carrying a modulation symbol. M OFDM symbols are combined into an OFDM frame. The transmitted modulation symbols in an OFDM frame can be represented as a matrix called the transmitted frame matrix. The modulation symbol at the kth subcarrier in the lth OFDM symbol of a transmitted OFDM frame is denoted as

$$(\mathbf{F}_{\text{Tx}})_{k,l} = a_{k,l}. \tag{1}$$

By OFDM processing [26], the received modulation symbol at the kth subcarrier in the lth OFDM symbol of a received OFDM frame is expressed as

$$
\begin{aligned}
(\mathbf{F}_{\text{Rx}})_{k,l} \\
= \sum_{h=0}^{H-1} \left\{ (\mathbf{F}_{\text{Tx}})_{k,l} \cdot b_h \cdot e^{-j2\pi T_o f_{D,h} l} \cdot e^{-j2\pi \tau_h (k\Delta f)} \cdot e^{j\varphi_n} \right\},
\end{aligned} \tag{2}
$$

where $\mathbf{F}_{\text{Rx}}$ is the received frame matrix consisting of H target returns, and Δf is the subcarrier spacing. $b_h, f_{D,h}, \tau_h$, and φ_h are complex amplitude, Doppler shift, round-trip time, and random phase rotation, respectively, associated with the hth target returns in a frame. The details of the above parameters can also be found in [26].

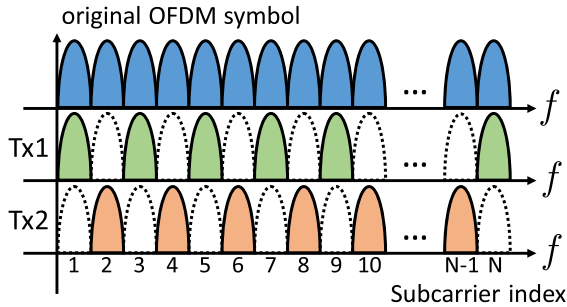**FIGURE 1.** Illustration of a collocated ULA-MIMO radar.

FIGURE 2. Illustration of spectrally interleaved subcarrier allocation.

B. ULA-MIMO-OFDM RADAR MODEL

Without loss of generality, we consider a collocated MIMO radar model, where there is a ULA with N_T transmit and N_R receive antennas. The transmit antennas and receive antennas are deployed with uniform spacing d_T and d_R respectively as shown in FIGURE 1. The antenna patterns follow the spec. of TI AWR1642BOOST-ODS evaluation board, which comes with a patch antenna [27]. In a MIMO radar system, the transmit antennas must radiate mutually orthogonal signals. In this paper, we propose to use spectrally interleaved OFDM signals, in which N_T mutually orthogonal signals are generated by spectrally dividing the original OFDM signal with interleaved subcarrier allocation illustrated in FIGURE 2.

The orthogonality of signals from the transmit antennas enables the receiver to distinguish signals from different transmit antennas, so a MIMO radar can be viewed as an augmented passive array radar [28]. Here we set $d_T = 2\lambda_c$ as $N_R d_R$ to form a contiguous $N_T N_R$-element virtual array uniformly spaced by d_R as shown in FIGURE 1. For example, a 2×4 MIMO radar configuration is equivalent to a virtual 8-element array radar. With spectrally interleaved MIMO-OFDM signals, the received modulation symbol at the kth subcarrier in the lth OFDM symbol at the ith virtual receive antenna can be represented as

$$\left[(\mathbf{F}_{\mathrm{Rx}})_i\right]_{k,l} = \sum_{h=0}^{H-1} \left\{ \begin{array}{l} (\mathbf{F}_{\mathrm{Tx}})_{k,l} \cdot b_h \\ \cdot e^{-j\pi i \frac{f_0 + (k-1)\Delta f}{f_c} \sin\theta_h} \\ \cdot e^{-j2\pi T_o f_{D,h} l} \cdot e^{-j2\pi \tau_h (k\Delta f)} \cdot e^{j\varphi_h} \end{array} \right\} + (\mathbf{W}_i)_{k,l}, \quad (3)$$

where f_0 is start frequency, and $\mathbf{W}_i$ is an AWGN matrix.

With the predetermined transmitted frame matrix $\mathbf{F}_{\mathrm{Tx}}$, the channel coefficient matrix (CCM) of each Tx/Rx antenna
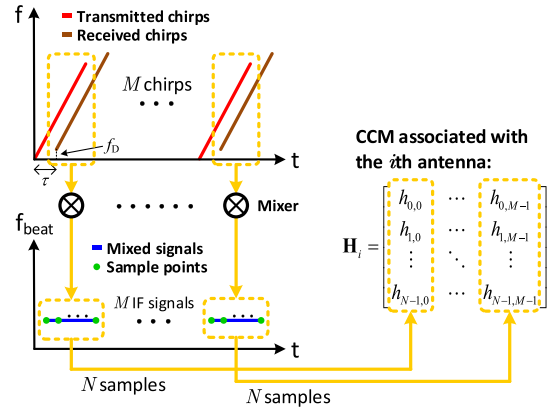

FIGURE 3. Illustration of CCM generation for FMCW radars.

pair can be obtained and represented as

$$[\mathbf{H}_i]_{k,l} = \frac{[(\mathbf{F}_{\mathrm{Rx}})_i]_{k,l}}{(\mathbf{F}_{\mathrm{Tx}})_{k,l}} = \left\{ \sum_{h=0}^{H-1} b_h e^{-j\pi i \frac{f_0 + (k-1)\Delta f}{f_c} \sin\theta_h} \right. \\ \left. e^{-j2\pi T_o f_{D,h} l} e^{-j2\pi \tau_h (k\Delta f)} e^{j\varphi_h} \right\} \\ + \left(\tilde{\mathbf{W}}_i\right)_{k,l}, \quad i = 1, 2, \ldots, N_T N_R, \quad (4)$$

where $\tilde{\mathbf{W}}_i$ is an AGWN matrix given that all modulation symbols have equal power, which is assumed in this paper. Note that the CCM reflects channel effect on target returns at different points in the T-F grid of the receiver. Moreover, range and Doppler velocity of a target induce phase differences between rows and columns of a CCM.

The above procedure for obtaining the CCMs also applies to FMCW radars because FMCW radars share nearly the same signal processing framework with OFDM radars as illustrated in FIGURE 3. It has been shown that the CCMs of FMCW radars are equivalent to those of OFDM radars when the frequency slope of FMCW chirps is sufficiently large [29].

C. 2D FFT OPERATION

The objective of the two-dimensional (2D) FFT operation is to acquire target information (i.e. range and Doppler velocity) from radar target returns. For the case of identifying sinusoids in a discrete-time signal, 2D FFT is the optimal solution if the sinusoids in the signals are well resolved. A CCM range-Doppler (RD) map is generated by 2D FFT for the CCM at the ith antenna, which can be represented as

$$2\mathrm{D\ FFT}\,(\mathbf{H}_i)\,(n, m) \\ = \sum_{k=0}^{N_{\mathrm{FFT}}-1} \left(\sum_{\mu=0}^{M_{\mathrm{FFT}}-1} (\mathbf{H}_i)_{k,l}\, e^{-j2\pi \frac{lm}{M_{\mathrm{FFT}}}} \right) e^{j2\pi \frac{kn}{N_{\mathrm{FFT}}}}, \\ i = 1, 2, \ldots, N_T N_R, \quad (5)$$

where N_{FFT} and M_{FFT} are the FFT lengths in the subcarrier and OFDM symbol domains respectively, and are given by $N_{\mathrm{FFT}} = N$ and $M_{\mathrm{FFT}} = M$.

A CCM RD map is composed of $N_{\mathrm{FFT}} \times M_{\mathrm{FFT}}$ *CCM RD bins*. Maximum-ratio-combining (MRC) is achieved at
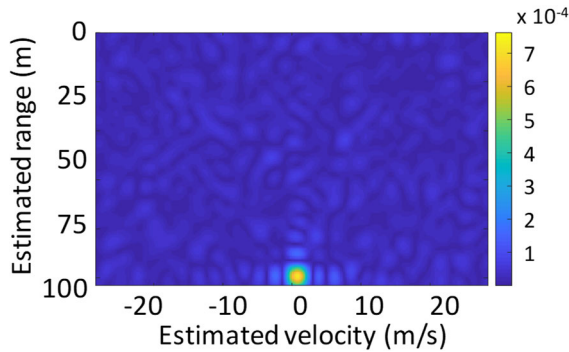
FIGURE 4. 2D CCM RD map with range = 100 m, Doppler velocity = 1.4 m/s, N = 256, M = 256, NFFT = 4096, MFFT = 4096, and SNR = 0 dB.

CCM RD bins when range and Doppler velocity of targets match both discrete sinusoidal components in both domains. They are called *MRC-CCM RD bins*, and yield local maxima in the CCM RD map as illustrated in FIGURE 4. There are remaining phase differences of the MRC-CCM RD bins between different antennas due to inter-antenna spacing and DOA of targets. Based on the phase differences, DOA of targets can be estimated. More importantly, a processing gain of $10\log_{10}(NM)$ dB can be achieved by MRC to enhance DOA estimation performance.
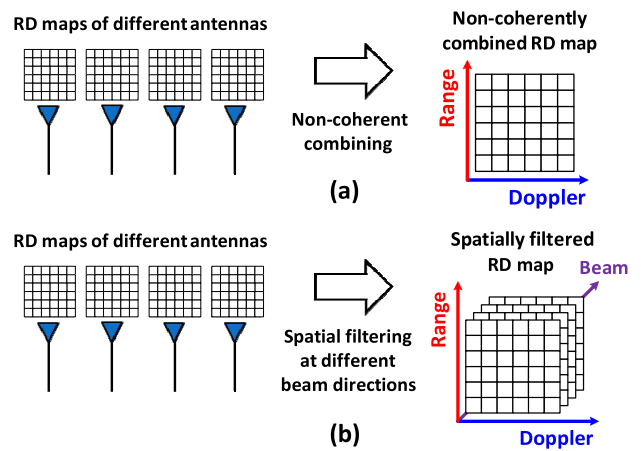
D. CFAR DETECTION IN MIMO RADARS

The idea of CFAR is to evaluate the average power of noise level according to neighboring cells surrounding the CUT and set an appropriate threshold for the detection. Moreover, for a given noise level and threshold, CFAR detection improves with high receive SNR of target returns (i.e., a high detection rate can be obtained). The receive SNR is defined as SNR observed at the receive antennas before the 2D FFT operation.

For noise level estimation with multiple antennas, a conventional way is to take the average of magnitude of CCM RD maps at different antennas. This is called *non-coherent combining* and it yields a *non-coherently combined RD map* as illustrated in FIGURE 5(a). The value at a certain RD bin in the non-coherently combined RD map is the average of the magnitudes of the values at the same RD bin of the individual RD maps at different antennas.

For target detection, as an alternative to the non-coherently combined RD map, a coherently combined RD map can improve CFAR detection with *spatial filtering*. The spatial filtering operation focuses CCM RD maps at different antennas to specific beam directions to enhance the power of target returns. It does not increase noise power because noise is non-directional. Ideally, the receive SNR of target returns can be enhanced by a factor of the number of antennas. The spatially filtered RD map at the sth beam direction is defined by

$$SFM_s(n, m) = \sum_{i=0}^{N_T N_R - 1} \text{2D FFT } (\mathbf{F}_i)(n, m) e^{j\pi i \frac{f_0 + (n-1)\Delta f}{f_c} \sin\theta_s},$$

$$s = 1, \ldots, S, \quad (6)$$

FIGURE 5. Illustration of (a) non-coherent combining and (b) spatial filtering in a MIMO radar system.

where S is the number of beam directions. With spatial filtering employed, CFAR detection can improve its detection rate because the receive SNR of target returns is enhanced by a factor of $N_T N_R$. FIGURE 5(b) gives the illustration of spatial filtering.

The above process requires that targets are detected based on S spatially filtered RD maps, leading to 3D CFAR detection, as illustrated in FIGURE 5(b). Compared to the process with a non-coherently combined RD map, which is 2D CFAR detection, 3D CFAR detection incurs higher complexity. This prompts the development of a low complexity version of 3D CFAR detection.

E. BASIC ASSUMPTIONS

The validity of the above signal models implies five assumptions as follows:

(E1) No distortion other than AWGN is induced by the transmit and receive front-ends.

(E2) The OFDM cyclic prefix (CP) duration is larger than the round-trip propagation time of the farthest target.

(E3) The subcarrier spacing is at least one order of magnitude larger than the largest Doppler shift.

(E4) The Doppler shift is the same at all subcarriers.

(E5) The target's distance and relative velocity to observer remain constant during the transmission of a single frame.

III. LOW-COMPLEXITY 3D CFAR DETECTION

In 3D CFAR detection, with more beam directions, there is a higher probability of pointing at the true target direction and achieving higher receive SNR of target returns. However, this will increase complexity according to (6). As a remedy, we propose a new technique to reduce complexity of 3D CFAR detection. The technique transforms a 3D CFAR detection into two simple 1D CFAR detections and a cross validation operation. It is described in three steps as follows:
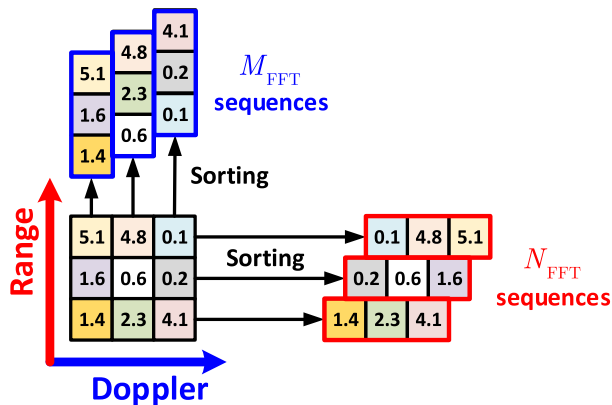
FIGURE 6. Illustration of sorting operation on non-coherently combined RD map.

A. STEP 1: THRESHOLD DETERMINATION

We sort the values of the non-coherently combined RD map in descending order along each row and column of the map respectively into $(N_{FFT} + M_{FFT})$ sequences, as shown in (7) and FIGURE 6 for an example.

$$\begin{cases} X_i(1) \geq \cdots \geq X_i(M_{FFT}), & i = 1, \ldots, N_{FFT} \\ X_i(1) \geq \cdots \geq X_i(N_{FFT}), & i = N_{FFT}+1, \ldots, N_{FFT}+M_{FFT}. \end{cases}$$
(7)

Then the estimated noise level E_i and threshold T_i are defined as in (8) for the ith sequence:

$$\begin{cases} E_i = X_i(k_i) \\ T_i = G \times E_i, \end{cases}, i = 1, \ldots, N_{FFT} + M_{FFT},$$
(8)

where G is a scaling factor to maintain a constant false alarm rate for target detection. The index k_i is chosen to be the smallest number that satisfies

$$\sum_{n=k_i}^{k_i+\beta-1} u\left(\frac{X_i(n)}{X_{i+1}(n)} - \alpha\right) = 0, \quad i = 1, \ldots, N_{FFT}+M_{FFT}, \quad (9)$$

where $u(\bullet)$ is the *unit step function*, α is the ratio threshold between adjacent values in a sequence, and β is a predetermined stop threshold. The goal of (9) is to select an index that represents the *elbow point* of a sorted sequence [30]. Specifically, a sorted sequence associated with target returns is composed of a steep sequence and a smooth sequence. An elbow point is defined as the end and start point of a steep and smooth sequences, respectively, as shown in FIGURE 7, in which $\beta = 3$ consecutive ratios of adjacent values are lower than α. The steep sequence usually contains power of target returns. Hence, based on the characteristic of smooth variation of noise power in a sorted sequence, choosing proper α and β can prevent the noise level E_i from being overestimated by taking power of target returns into account. For the considered environment, choosing $\alpha = 1$ dB and $\beta = 10$ yields robust noise level estimation. Finally, we can
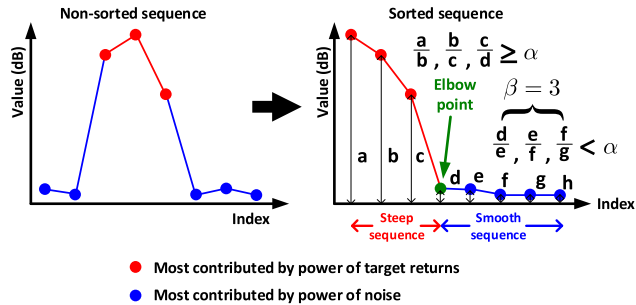

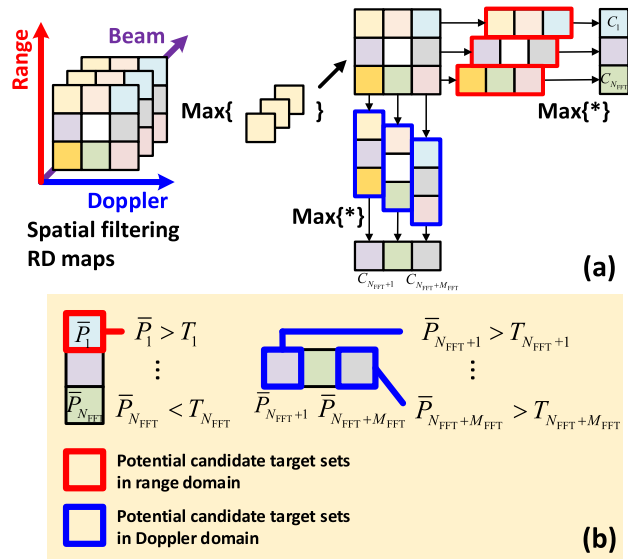**FIGURE 7. Illustration of CFAR threshold determination.**

FIGURE 8. Illustration of (a) maximum operation (b) two 1D CFAR detections in candidate target set determination.

obtain the thresholds for all rows of the non-coherently combined RD map as $\{T_1, T_2, \ldots, T_{N_{FFT}}\}$ and all columns as $\{T_{N_{FFT}+1}, T_{N_{FFT}+2}, \ldots, T_{N_{FFT}+M_{FFT}}\}$.

B. STEP 2: CANDIDATE TARGET SET DETERMINATION

After determining the threshold for each row and column of the non-coherently combined RD map, candidate target sets in range and Doppler domains can be determined. First, we take the maximum value of S spatially filtered RD maps for the CCM RD bin at the rth row and cth column and record the corresponding beam direction index, and denote them as $(P_{r,c}, \text{id}_{r,c})$, where $r = 1, \ldots, N_{FFT}$ and $c = 1, \ldots, M_{FFT}$. As shown in FIGURE 8(a), a *maximum RD map* is constructed.

The above maximum taking operation helps retain spatial improvement of receive SNR of target returns, and reduce the complexity of 3D CFAR detection. For further complexity reduction, the same operation is applied to the *maximum RD map* in range and Doppler domains to acquire two sequences $\{\bar{P}_1, \ldots, \bar{P}_{N_{FFT}}\}$ and $\{\bar{P}_{N_{FFT}+1}, \ldots, \bar{P}_{N_{FFT}+M_{FFT}}\}$, whose elements are maximum values of rows or columns of the maximum RD map. Their corresponding beam direction index

sets are $\{\overline{\overline{id}}_1, \ldots, \overline{\overline{id}}_{N_{\mathrm{FFT}}}\}$ and $\{\overline{\overline{id}}_{N_{\mathrm{FFT}}+1}, \ldots, \overline{\overline{id}}_{N_{\mathrm{FFT}}+M_{\mathrm{FFT}}}\}$. The procedure outline in III.A and III.B transforms a 3D CFAR detection into two 1D CFAR detections with much lower complexity. For the 1D CFAR detection, as shown in FIGURE 8(b), a target is declared at the ith CUT if $P_{ig} > T_i$ is true, where $r = 1, \ldots, N_{\mathrm{FFT}} + M_{\mathrm{FFT}}$. Assuming there are I and J targets declared in range and Doppler domains respectively, their range and Doppler velocity can be expressed as $\{\hat{d}_1, \ldots, \hat{d}_I\}$ and $\{\hat{v}_1, \ldots, \hat{v}_J\}$. Their corresponding beam direction index sets are $\{\tilde{id}_{\mathrm{d},1}, \ldots, \tilde{id}_{\mathrm{d},I}\}$ and $\{\tilde{id}_{\mathrm{v},1}, \ldots, \tilde{id}_{\mathrm{v},J}\}$.

C. STEP 3: CROSS VALIDATION

The final target list is confirmed by a cross validation to check CUTs with index pair (d_i, v_j) using of the 2D OS-CFAR technique [8], where $i = 1, \ldots, I$ and $j = 1, \ldots, J$. There are IJ candidate targets to be checked. Assuming U targets are declared by the cross validation, the final parameter set of targets is $\{(\hat{d}_1, \hat{v}_1, \hat{\theta}_1), \ldots, (\hat{d}_U, \hat{v}_U, \hat{\theta}_U)\}$.

D. SUMMARY

The proposed CFAR detection converts the high complexity 3D CFAR detection into (1) maximum RD map generation, (2) two 1D CFAR detections and (3) DOA estimation (to be discussed in the next section). The overall complexity is greatly reduced. There may be a certain increase in latency due to the more steps involved. Fortunately, the two 1D CFAR detections can be performed in parallel, and the other two steps are single-shot operations and do not incur much extra latency to the proposed method.

IV. ESPRIT BASED DOA ESTIMATION

After the above CFAR detection, U estimated target parameter sets (i.e. $(\hat{d}_u, \hat{v}_u, \hat{\theta}_u) \in \Omega_U$) associated with U MRC-CCM RD bins can be obtained. The accuracy and resolution of $\hat{d}_u$ and $\hat{v}_u$ depend on the aperture size in frequency and time domains respectively (i.e., number of subcarriers, N, and number of OFDM symbols in a frame, M). With modern OFDM and Sample-and-Hold circuits, N and M are typically large enough to achieve high accuracy and resolution of range and velocity. In comparison, the resolution and accuracy of DOA estimation is restricted by the limited aperture size in the spatial domain. It is thus possible that more than one target is present at the same MRC-CCM RD bin and not detected by the low-complexity 3D CFAR detection.

In this section, we propose a T-F division signal preprocessing operation to generate multiple snapshots for DOA estimation. Spatial and frequency decorrelation is then exploited to decorrelate coherent target returns. Next, a modified ESPRIT based DOA estimation technique without preliminary knowledge of target number is proposed. For brevity, in this section, the processing flow will be demonstrated for the uth target parameter set $(\hat{d}_u, \hat{v}_u, \hat{\theta}_u)$ at the uth MRC-CCM RD bin. The technique can be divided into three steps as illustrated in FIGURE 9, and are introduced in the following subsections.
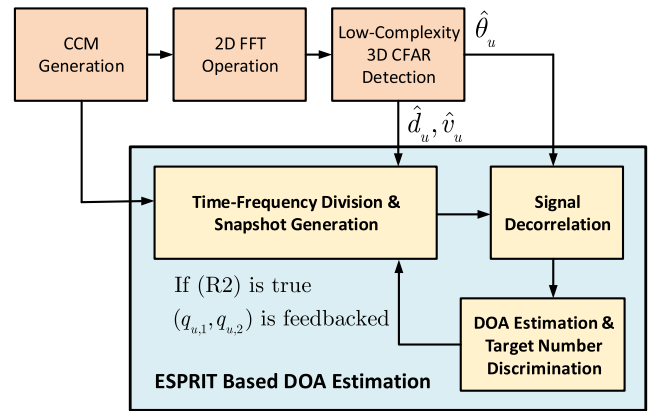
FIGURE 9. Block diagram of proposed ESPRIT based DOA estimation technique.

A. STEP 1: TIME-FREQUENCY DIVISION AND SNAPSHOT GENERATION

$N_{\mathrm{T}}N_{\mathrm{R}}$ CCMs are acquired from a frame of OFDM radar signal return with bandwidth B. A CCM is evenly divided into N_{divide} and M_{divide} parts in frequency and time domains, respectively, and generate $N_{\mathrm{divide}}M_{\mathrm{divide}}$ *channel coefficient sub-matrices (CCSMs)* in the CCM. The mth CCSM associated with the ith antenna is denoted as
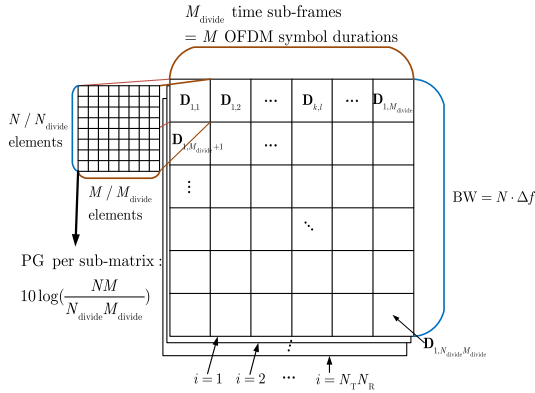
$$\mathbf{D}_{i,m} \in \mathbb{C}^{N/N_{\mathrm{divide}} \times M/M_{\mathrm{divide}}}, \quad m = 1, 2, \ldots, N_{\mathrm{divide}}M_{\mathrm{divide}}, \quad (10)$$

and $\mathbf{D}_{i,m}$ belongs to the pth sub-band for $m = (p-1)M_{\mathrm{divide}} + 1, \ldots, pM_{\mathrm{divide}}$. Following the same concept in II.D, an CCSM RD map is composed of $(N/N_{\mathrm{divide}}) \times (M/M_{\mathrm{divide}})$ CCSM RD bins. U MRC-CCSM RD bins of a CCSM RD map can be found by a 2D FFT operation. For each antenna, $N_{\mathrm{divide}}M_{\mathrm{divide}}$ *snapshots* are defined as the values of the uth MRC-CCSM RD bins in $N_{\mathrm{divide}}M_{\mathrm{divide}}$ CCSM RD maps, leading to $N_{\mathrm{divide}}M_{\mathrm{divide}}$ 2D FFT operations to obtain target parameter sets associated with the CCSM RD maps. High computational cost is thus induced.

To reduce the computational cost, with assumption (E5), we exploit the target parameter sets given from the previous stage (CFAR stage) to generate the snapshots. For the uth MRC-CCSM RD bins in CCSM RD maps, we can substitute the target parameter set $(\hat{d}_u, \hat{v}_u, \hat{\theta}_u)$ and the mth CCSM at ith antenna into (11) to acquire the ith element of the mth snapshot vector at low computational cost, where the snapshot vector is defined by (12).

$$s_{u,i,m} = \sum_{k=0}^{N/N_{\mathrm{divide}}-1} \left(\sum_{l=0}^{M/M_{\mathrm{divide}}-1} (\mathbf{D}_{i,m})_{k,l} \cdot e^{-j2\pi \frac{\hat{v}_u}{v_{\mathrm{max}}} l} \right) e^{j2\pi \frac{\hat{d}_u}{d_{\mathrm{max}}} k}, \quad (11)$$

$$\mathbf{s}_{u,m} = [s_{u,1,m}, s_{u,2,m}, \ldots, s_{u,N_{\mathrm{T}}N_{\mathrm{R}},m}]^T. \quad (12)$$

FIGURE 10. Illustration of T-F division operation. $N_{\text{divide}}M_{\text{divide}}$ CCSMs are obtained by equally dividing each CCM at each antenna according to the selected N_{divide} and M_{divide}.

Then, we can have a snapshot matrix for the uth target in the pth subband given by

$$\mathbf{S}_{u,p} = [\mathbf{s}_{u,1+(p-1)M_{divide}}, \mathbf{s}_{u,2+(p-1)M_{divide}}, \ldots, \mathbf{s}_{u,pM_{divide}}]$$
$$\in \mathbb{C}^{N_T N_R \times M_{divide}}. \quad (13)$$

Consider a ULA with $N_T N_R$ identical antennas $\{1,\ldots, N_T N_R\}$ divided into overlapping subarrays of size N_{sub} (where $N_{\text{sub}} \leq N_T N_R$) with antennas $\{1,\ldots, N_{\text{sub}}\}$ forming the first subarray, antennas $\{2,\ldots, N_{\text{sub}} + 1\}$ forming the second subarray, etc. The snapshot sub-matrix of the lth sub-array for the uth detected target can be defined as

$$\mathbf{S}_{u,p,l}$$
$$= [\mathbf{0}_{N_{\text{sub}} \times (l-1)} | \mathbf{I}_{N_{\text{sub}} \times N_{\text{sub}}} | \mathbf{0}_{N_{\text{sub}} \times (L-l)}]^H_{N_{\text{sub}} \times N_T N_R}$$
$$\cdot [\mathbf{s}_{u,1+(p-1)M_{divide}}, \mathbf{s}_{u,2+(p-1)M_{divide}}, \ldots, \mathbf{s}_{u,pM_{divide}}]_{N_T N_R \times M_{divide}}$$
$$= \mathbf{A}(f_p, \theta_u)\mathbf{X}_{u,p,l} + \mathbf{Z}_{u,p,l}$$
$$= [\mathbf{x}_{u,p,l}(1), \mathbf{x}_{u,p,l}(2), \ldots, \mathbf{x}_{u,p,l}(M_{\text{divide}})]. \quad (14)$$

where $\mathbf{I}_{Q \times Q}$ and $\mathbf{O}_{Q \times W}$ are the identity and zeros matrices of a proper size, and $L = N_T N_R - N_{\text{sub}} + 1$. $\mathbf{A}(f, \boldsymbol{\theta}_u)$ is the $N_{\text{sub}} \times D$ direction matrix composed of D steering vectors at frequency f associated with the DOAs, where D is the number of targets at the uth MRC-CCM RD bin. $\mathbf{X}_{u,p,l}$ is the $D \times M_{\text{divide}}$ signal matrix composed of D rows of coherent signal vectors, and $\mathbf{Z}_{u,p,l}$ is the $N_{\text{sub}} \times M_{\text{divide}}$ AWGN matrix. The spatial covariance matrix in the pth subband at the lth subarray can be represented as

$$\mathbf{R}_{u,p,ll} = \mathrm{E}\left[\mathbf{x}_{u,p,l}(n)\mathbf{x}^H_{u,p,l}(n)\right] \simeq \mathbf{S}_{u,p,l}\mathbf{S}^H_{u,p,l}/M_{\text{divide}}. \quad (15)$$

For the choice of N_{divide} and M_{divide}, a rule of thumb is that $N_{\text{divide}}M_{\text{divide}}$ should be at least $2N_T N_R$ to ensure accurate estimation of the covariance matrix. N_{divide} should be large enough to maintain the narrowband assumption for each CCSM. For a larger M_{divide}, more effective snapshots can be obtained, which will be elaborated in IV.B. FIGURE 10 illustrates the proposed T-F division operation.

B. STEP 2: TARGET DECORRELATION

For the uth target, with N_{divide} snapshot matrices in each subband, we can acquire a full-size sample spatial covariance matrix of size $(N_T N_R) \times (N_T N_R)$, and employ a high-resolution subspace based DOA estimation technique. However, such a technique would fail to resolve multiple targets whose returns are coherent due to that they are emitted from the same radar transmitter. In the following, we adopt a preprocessing operation to decorrelate the coherent returns, which includes spatial smoothing, frequency smoothing, and forward-backward averaging [18]–[20].

1) SPATIAL SMOOTHING (SS)

We first partition the array into L subarrays and then generate the average of the subarray spatial covariance matrices to decorrelate coherent target returns [18]. The spatial covariance matrix after spatial smoothing in the pth subband for the uth target is formed by

$$\mathbf{R}_{u,p} = \sum_{l=1}^{L} \hat{\mathbf{R}}_{u,p,l}/L, \quad (16)$$

where $\hat{\mathbf{R}}_{u,p,l} = \mathbf{S}_{u,p,l}\mathbf{S}^H_{u,p,l}/M_{\text{divide}}$.

2) FREQUENCY FOCUSING (FF)

When working with a large signal bandwidth, the direction matrix may vary with frequency. In this case, we can focus the direction matrix at frequency f_p into the one at frequency f_c by designing a focusing matrix $\mathbf{T}(f_p)$ that satisfies

$$\mathbf{T}(f_p)\mathbf{A}(f_p, \theta) = \mathbf{A}(f_c, \theta), \quad p = 1, 2, \ldots, N_{\text{divide}}. \quad (17)$$

A plausible solution to focusing is the Rotational Signal Subspace (RSS) given by $\mathbf{T}(f_p) = \mathbf{U}(f_p)\mathbf{V}^H(f_p)$[18], where the columns of $\mathbf{U}(f_p)$ and $\mathbf{V}(f_p)$ are the left and right singular vectors of $\mathbf{A}(f_c, \bar{\theta})\mathbf{A}(f_p, \bar{\theta})^H$. $\bar{\theta}$ is a set of preselected angles consisting of preliminary coarse DOA estimates $\hat{\theta}_u$ associated with the uth MRC-CCM RD bin and two auxiliary angles $(\hat{\theta}_u \pm 0.25 \, \text{BW}_{\text{3dB}})$ [31], where BW_{3dB} is the 3-dB beam width of the array. The focused covariance matrix is defined as

$$\mathbf{R}_u = \sum_{p=1}^{N_{\text{divide}}} \mathbf{T}(f_p)\mathbf{R}_{u,p}\mathbf{T}^H(f_p). \quad (18)$$

Frequency focusing is also shown to be effective in decorrelating coherent signals [31].

3) FORWARD-BACKWARD AVERAGING (FBA)

To further enhance decorrelation, the FBA operation [19] is adopted, which leads to the FBSS-FF spatial covariance matrix given by

$$\mathbf{R}_{u,\text{FBA}} = \frac{1}{2}\left(\mathbf{R}_u + \mathbf{J}\mathbf{R}^*_u\mathbf{J}\right), \quad (19)$$

where $\mathbf{J}$ is a matrix containing ones in its anti-diagonal and zeros elsewhere.

C. STEP 3: DOA ESTIMATION AND TARGET NUMBER DISCRIMINATION

In practice, it is unlikely that more than two targets with different DOAs share the same range and Doppler velocity estimates (i.e., falling into the same CCM RD bin) because of the limitation of FOV of radars, and the size of vehicles. Assuming that there are at most two targets at each MRC-CCM RD bin, we propose a modified ESPRIT based technique as follows.

Denote as $\bar{D}$ a guess of target number. By applying ESPRIT with $\bar{D} = 1$, we obtain (q_u, λ_u), where q_u and λ_u are the estimated DOA and corresponding eigenvalue respectively. With $\bar{D} = 2$, we obtain $(q_{u,1}, \lambda_{u,1})$ and $(q_{u,2}, \lambda_{u,2})$. By comparing the results with $\bar{D} = 1$ and $\bar{D} = 2$, the target number $\hat{D}$ and DOA can be jointly determined by the following criterion as summarized in (20). The detailed derivation of the criterion which is available online can be found in [32].

$$
\begin{cases}
\hat{D} = 2, \ \text{take} q_{u,1} \text{ and } q_{u,2}, \\
\quad \text{if} \left(|\lambda_u - \lambda_{u,1}| \geq \varepsilon_1, |\lambda_u - \lambda_{u,2}| \geq \varepsilon_1 \right) \\
\quad \text{or} \left(|\lambda_u - \lambda_{u,1}| \leq \varepsilon_2, |\lambda_u - \lambda_{u,2}| \leq \varepsilon_2 \right) \\
\quad \text{or} \left(||\lambda_u| - 1| \leq \varepsilon_3, ||\lambda_{u,1}| - 1| \leq \varepsilon_3, ||\lambda_{u,2}| - 1| \leq \varepsilon_3 \right) \\
\hat{D} = 1, \ \text{take } q_u, \ \text{otherwise,}
\end{cases}
$$
(20)

where ε_1, ε_2 and ε_3 are predetermined thresholds.

Finally, an additional confirmation of $\hat{D} = 2$ is conducted. $q_{u,1}$ and $q_{u,2}$ are taken as DOA estimates (i.e., $\hat{D} = 2$) if one of the following two requirements is satisfied.

(R1) the angle difference $|q_{u,1} - q_{u,2}|$ is smaller than $\text{BW}_{3\text{dB}}$.

(R2) the angle difference $|q_{u,1} - q_{u,2}|$ is larger than $\text{BW}_{3\text{dB}}$, and $q_{u,1}$ and $q_{u,2}$ correspond to peaks of beam response at the uth MRC-CCM RD bin.

Otherwise, q_u is taken as the DOA estimate ($\hat{D} = 1$). If (R2) is confirmed, $q_{u,1}$ and $q_{u,2}$ are taken as preliminary coarse DOA estimates and the procedure in step 2 is repeated, which yields better focusing matrices to further enhance DOA estimation. The proposed ESPRIT based DOA estimation technique is summarized in PSEUDO CODE I.

As a final remark, if the assumption of no more than two targets at each MRC-CCM RD bin is not met, then the target number will be most likely decided as 2, and the resulting DOA estimates will be some weighted averages of the target DOAs, according to the property of ESPRIT. To cope with the rare case of more than two targets, extra conditions and/or multiple frames can be incorporated in the criterion [32].

V. SIMULATION RESULTS

The simulation environment is based on MATLAB 2018a on a computer with an Intel i7-3770 CPU Core and 32GB of memory. In all simulations, a 2×4 MIMO-OFDM radar system as depicted in FIGURE 1 with an SRR waveform characteristic is considered according to commercial SRR designs and hardware specifications [34], [27]. TABLE 1 shows the general parameter setting.

Pseudo Code 1 Proposed ESPRIT Based DOA Estimation Technique

Inputs: $\mathbf{F}_i$, $i = 1, \ldots, N_T N_R$, $(\hat{d}_u, \hat{v}_u, \hat{\theta}_u)$, $u = 1, \ldots, U$
Outputs: $(\hat{d}_w, \hat{v}_w, \hat{\vartheta}_w)$, $w = 1, \ldots, W$
* **STEP 1 starts** and set $W = 0$
Acquire $\mathbf{D}_{i,m}$ by $\mathbf{F}_i$
FOR $u = 1, \ldots, U$
    Calculate $s_{u,i,m}, \mathbf{s}_{u,m}, \mathbf{S}_{u,p}, \mathbf{S}_{u,p,l}$ by (11)-(14);
END
***STEP 1 ends**;
FOR $u = 1, \ldots, U$ (default $W = 0$)
    flag_ReDO = 0;
    ***STEP 2 starts**
    Calculate $\mathbf{R}_{u,p,l}, \mathbf{R}_{u,p}, \mathbf{R}_u$ and $\mathbf{R}_{\text{FBA},u}$ by (16)-(19);
    ***STEP 2 ends / STEP 3 starts**
    Acquire (q_u, ϕ_u, λ_u), $(q_{u,1}, \phi_{u,1}, \lambda_{u,1})$ and $(q_{u,2}, \phi_{u,2}, \lambda_{u,2})$;
    Obtain $\hat{D}$ and target DOA(s) by (20)
    IF $\hat{D} = 2$
        IF ((R2) is true) & (flag_ReDO = 0)
            flag_ReDO = 1;
            go back to STEP 2 and refocus at $q_{u,1}$ and $q_{u,2}$;
        ELSE $\hat{D} = 1$;
        END
    END
    FOR $w = W + 1, \ldots, W + \hat{D}$
        $w' = w - W$;
        IF $\hat{D} = 2$, $\bar{\theta}_{w'} = q_{u,w'}$;
        ELSE $\bar{\theta}_{w'} = q_u$;
        END
        $\hat{\vartheta}_w = \bar{\theta}_{w'}$; $(\hat{d}_w, \hat{v}_w) = (\hat{d}_u, \hat{v}_u)$;
    END
    $W = W + \hat{D}$;
    ***STEP 3 ends**
END

A. LOW-COMPLEXITY 3D CFAR DETECTION

In this subsection, we evaluate the performance of the proposed CFAR detection technique under the Weibull distribution clutter model [33]. For each simulation, we conduct 10,000 Monte Carlo experiments. In the following simulations, we compare the proposed 3D CFAR and conventional 2D OS-CFAR techniques [8] in terms of detection rate and computational complexity. Note that 2D OS-CFAR needs to exhaustively check all CUTs in the maximum RD map. The simulation settings are given in Table 2. There are two scenarios with different target range-Doppler distributions, as shown in FIGURE 11(a) and FIGURE 11(b). Targets are easier to be detected with random distribution as illustrated in FIGURE 11(a). On the other hand, rectangular distribution as shown in FIGURE 11(b) induces masking effect [35], leading to degradation in detection rate.

Denote as SNR_O the SNR observed at an MRC-CCM RD bin with spatial filtering, and SNR_I the receive SNR

TABLE 1. General parameters used in computer simulations.

| Parameters	Value
Carrier frequency, f_c	78 (GHz)
No. of beam directions, S	32
Field of view (FOV)	[-60, 60]
Effective array size, $N_T N_R$	8 (2T4R)
Antenna spacing, d_R ($d_T = N_R d_R$)	1.9 mm ($0.5\lambda_u = 0.5c/f_c$)
Bandwidth, B	1 (GHz)
Subcarrier spacing, Δf	976 (kHz)
OFDM symbol period, T_O	51 (us)
Frame period, T_F	26 (ms)
$N = N_{FFT}$	1024
$M = M_{FFT}$	256
Unambiguity range/ velocity	153.6 (m)/37.5 (m/s)
Range/ velocity resolution	0.15 (m)/0.15 (m/s)
RCS, σ_{RCS}	10 (m^2)
Scaling factor, G	15 (dB)

TABLE 2. Simulation Parameter Settings for Evaluating the Computational Complexity and Detection Rate of Proposed CFAR Detection Technique.

| Parameters	Value
Receive SNR (SNR$_I$) of targets	[-73:3:-13] (dB)
Clutter to noise ratio (CNR)	-∞, 10 (dB)
Ratio threshold and Stop threshold,α and β	1 (dB) and 10
Order (2D OS-CFAR) / number of guard and reference cells	20 / 4 / 8

as defined in Section II.D. We have $SNR_O \approx SNR_I + 10\log_{10}(NMN_T N_R) \approx SNR_I + 63$ dB. CNR is the ratio of clutter power over noise power at each RD bin. FIGUREs 12 and 13 show the comparison of detection rate with different target numbers and CNR for the two target distribution scenarios. As a rule of thumb, a target can be successfully detected when SNR_O is higher than 30-35 dB [36], and a typical value of CNR is 10 dB [37]. For all cases, the performance of the proposed technique can achieve that of 2D OS-CFAR with SNR_O higher than 30 dB. When SNR_O is lower than 30 dB, the proposed technique tends to overestimate noise level and hence has a lower detection rate than 2D OS-CFAR, and this is more significant when clutter is present. In the presence of clutter, both techniques degrade slightly and the proposed technique can still achieve the performance of 2D OS-CFAR with SNR_O higher than 30 dB. On the other hand, for the distribution shown in FIGURE 11(b), although severe masking effects occur, the proposed technique can still reach the performance of 2D OS-CFAR.
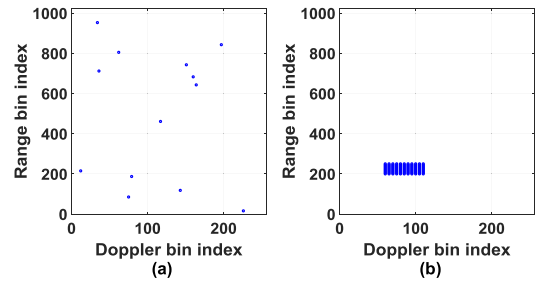
FIGURE 11. Target distribution scenarios: (a) random distribution (b) rectangular distribution.
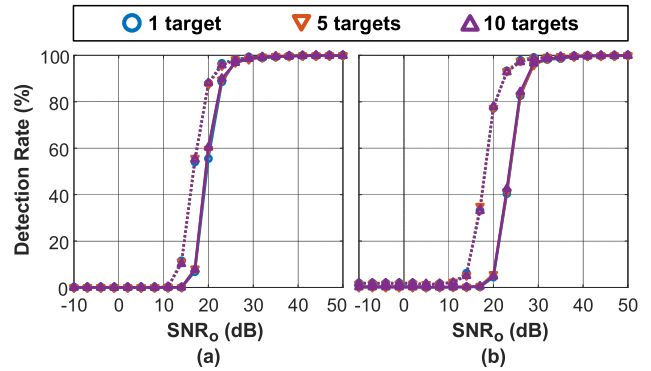
FIGURE 12. Detection rate in the random distribution scenario. Solid line: proposed technique; Dash line: 2D OS-CFAR. (a) CNR = −∞ dB (b) CNR = 10 dB.
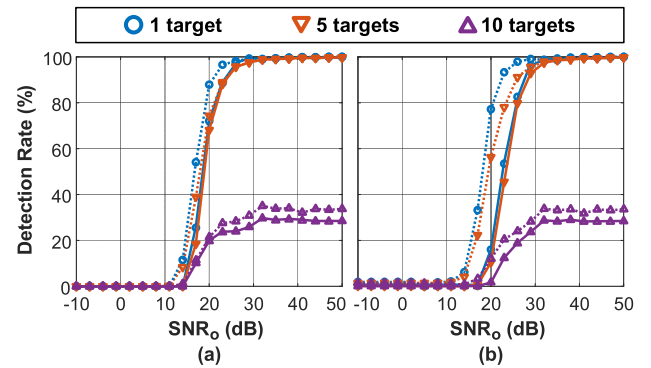
FIGURE 13. Detection rate in the rectangular distribution scenario. Solid line: proposed technique; Dash line: 2D OS-CFAR. (a) CNR = −∞ dB (b) CNR = 10 dB.

FIGUREs 14 and 15 show the comparison of computation time with different SNR_O and CNR for the two target distribution scenarios. The proposed technique requires only about 1% of the computation time of 2D OS-CFAR in the low SNR regime. In the high SNR regime, more candidate targets would be declared because of the relatively lower noise level. Thus, higher computational complexity is required to conduct more cross validations for the targets. In the presence of clutter, the proposed technique requires a longer computation time because more candidate targets would be declared.

B. ESPRIT BASED DOA ESTIMATION
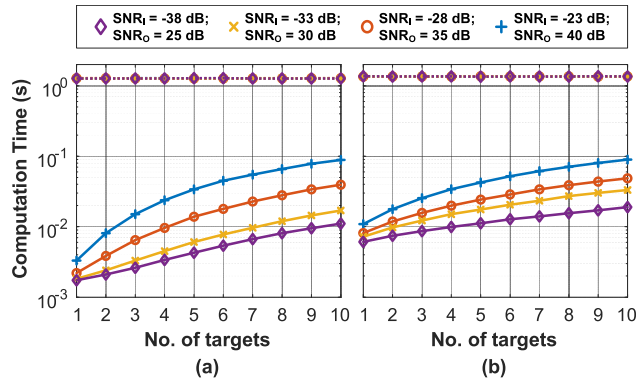In this subsection, we compare the performance of the proposed DOA estimation technique with existing techniques.

FIGURE 14. Computation time in the random distribution scenario. Solid line: proposed technique; Dash line: 2D OS-CFAR. (a) CNR $= -\infty$ dB (b) CNR $= 10$ dB.
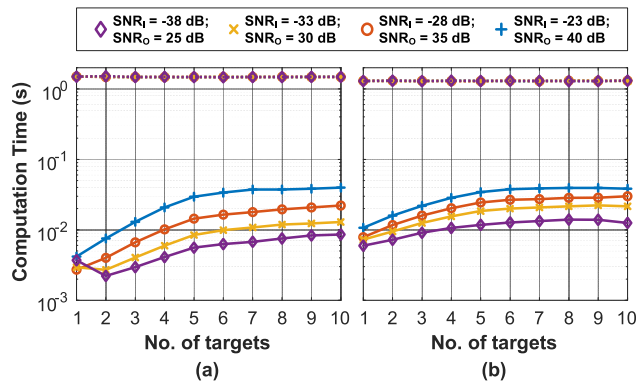

FIGURE 15. Computation time in the rectangular distribution scenario. Solid line: proposed technique; Dash line: 2D OS-CFAR. (a) CNR $= -\infty$ dB (b) CNR $= 10$ dB.

TABLE 3. Simulation parameter settings for evaluating the resolution probability and RMSE of proposed technique.

Parameters	Value
Receive SNR (SNR$_I$) of targets	-27, -17 (dB)
DOA of targets	$\pm$ 0.5, 1, 1.5, 2, 2.5 (°)
Subarray size, N_{sub}	7

We consider five different cases with two targets having the same range and Doppler velocity and separated by 1, 2, 3, 4 and 5 degrees. The simulation settings are given in Table 3. We conduct 1000 Monte Carlo experiments for each case to evaluate the performance of each technique. In all simulations, $\Delta\theta$ stands for the difference between the two targets' DOA.

1) EFFECT OF T-F RESOURCE DIVISION

As suggested in Section IV, for an 8-element array, a proper choice for the number of snapshots is 16. Different combinations of N_{divide} and M_{divide} lead to different degrees of decorrelation of SS and FF operations. FIGUREs 16 and 17 show the target resolution probability
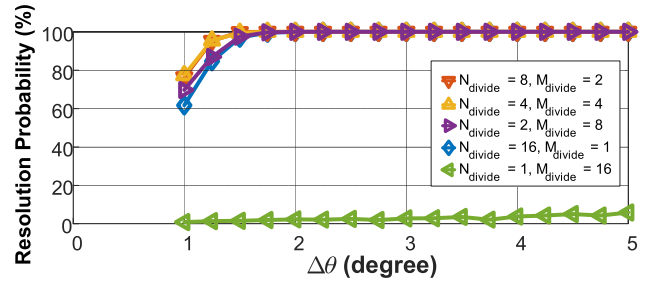

FIGURE 16. Comparison of resolution probability performance with different T-F division settings. SNR$_I$ = −17 dB (SNR$_\theta$ = 25 dB).
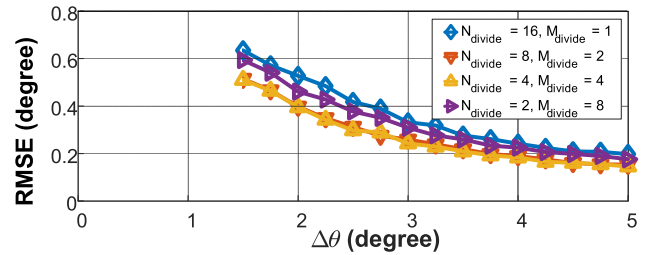

FIGURE 17. Comparison of RMSE performance with different T-F division settings. SNR$_I$ = −17 dB (SNR$_\theta$ = 25 dB).
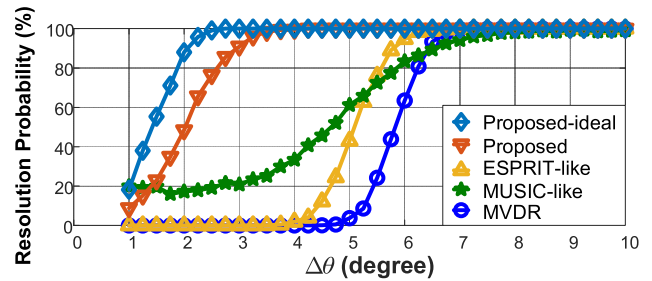

FIGURE 18. Comparison of resolution probability performance of different DOA estimation techniques with SNR$_I$ = −27 dB (SNR$_\theta$ = 15 dB).
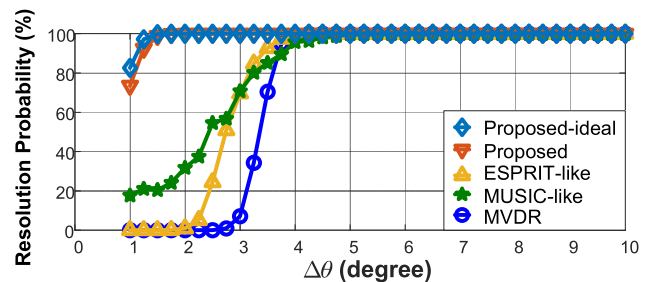

FIGURE 19. Comparison of resolution probability performance of different DOA estimation techniques with SNR$_I$ = −17 dB (SNR$_\theta$ = 25 dB).

and root-mean-square-error (RMSE) of the proposed DOA estimation technique with five different combinations and SNR$_I$ = −17 dB. For all cases, a processing gain of $10\log_{10}(NM/N_{\text{divide}}M_{\text{divide}}) \approx 42$ dB can be achieved, so the effective SNR (SNR$_\theta$) for DOA estimation is 25 dB. It is found that $N_{\text{divide}} = 8$, $M_{\text{divide}} = 2$ gives the best performance. In this case, the eight subbands satisfy the narrowband assumption with a moderate focusing error.
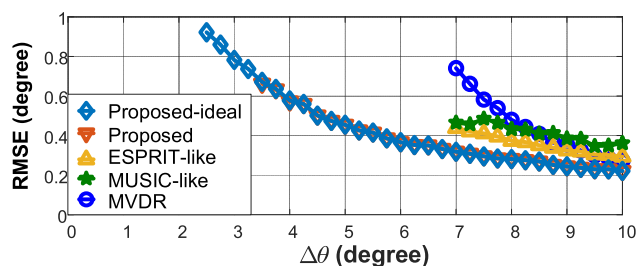
FIGURE 20. Comparison of RMSE performance of different DOA estimation techniques with $SNR_I = -27$ dB ($SNR_\theta = 15$ dB).

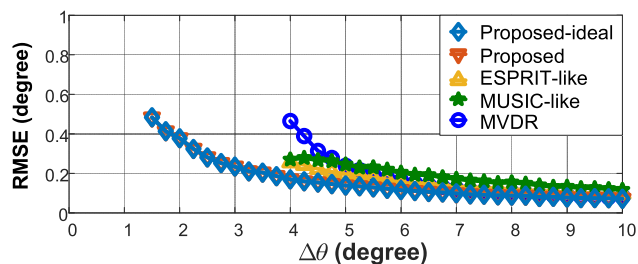**FIGURE 21.** Comparison of RMSE performance of different DOA estimation techniques with $SNR_I = -17$ dB ($SNR_\theta = 25$ dB).

2) PERFORMANCE COMPARISON WITH EXISTING TECHNIQUES

Here we compare the proposed DOA estimation technique with the MVDR [11], ESPRIT-like [24] and MUSIC-like [25] techniques. These techniques are chosen for comparison because they all provide high-resolution DOA estimation without knowledge of target number. For all techniques, the proposed T-F division and decorrelation operations are employed with $N_{\text{divide}} = 8$, $M_{\text{divide}} = 2$. As a benchmark, we also include the result of the proposed technique with perfect knowledge of target number, which we denote as proposed-ideal.

FIGUREs 18-21 show the target resolution probability and RMSE of the four techniques with different SNR_I. We can observe that the proposed technique outperforms the other three techniques with an angular resolution of 2 degrees and lower RMSE. As expected, the MVDR technique has the poorest performance compared to the other three subspace based techniques. The ESPRIT-like technique exhibits poorer resolution than the MUSIC technique because of reduction in effective array aperture. The MUSIC-like technique exploits the same array aperture as the proposed technique. However, its resolution degrades due to that only one noise eigenvector is used for computing the spatial power spectrum. Finally, the proposed technique performs equally well with and without knowledge of target number. This confirms the effectiveness of the proposed target discrimination criterion presented in Section IV.C.

VI. CONCLUSIONS

In this paper, we propose a parameter estimation method for MIMO radars. The method comprises a low-complexity CFAR target detection technique and an ESPRIT-based DOA

estimation technique that does not require knowledge of the target number. The CFAR detection technique leverages a spatial filtering operation to extend its coverage and performs low-complexity peak detection by converting the original 3D detection task into two 1D tasks. The DOA estimation technique adopts a proposed T-F division preprocessing operation to generate high-quality snapshots, as well as a criterion enabling ESPRIT to conduct DOA estimation without knowledge of the target number. The simulation results show that the proposed method significantly outperforms the conventional detectors in terms of complexity and angular resolution. In particular, it requires only 1% of the computational time of traditional 2D OS-CFAR with approximately the same detection rate.

REFERENCES

[1] A. G. Stove, "Linear FMCW radar techniques," *IEE Proc. F Radar Signal Process.*, vol. 139, no. 5, pp. 343–350, Oct. 1992.

[2] M. Skolnik, *Radar Handbook*, 3rd ed. New York, NY, USA: McGraw-Hill, 2008.

[3] I. V. Komarov and S. M. Smolskiy, *Fundamentals of Short-Range FM Radar*, 1st ed. Norwood, MA, USA: Artech House, 2003.

[4] H. Rohling and C. Moller, "Radar waveform for automotive radar systems and applications," in *Proc. IEEE Radar Conf.*, May 2008, pp. 1–4.

[5] M. Weiss, "Analysis of some modified cell-averaging CFAR processors in multiple-target situations," *IEEE Trans. Aerosp. Electron. Syst.*, vol. AES-18, no. 1, pp. 102–114, Jan. 1982.

[6] H. Rohling, "Radar CFAR thresholding in clutter and multiple target situations," *IEEE Trans. Aerosp. Electron. Syst.*, vol. AES-19, no. 4, pp. 608–621, Jul. 1983.

[7] H. Rohling and R. Mende, "OS CFAR performance in a 77 GHz radar sensor for car application," in *Proc. Int. Conf. Radar*, 1996, pp. 109–114.

[8] J. Yan, X. Li, and Z. Shao, "Intelligent and fast two-dimensional CFAR procedure," in *Proc. IEEE Int. Conf. Commun. Problem-Solving (ICCP)*, Guilinm, China, Oct. 2015, pp. 461–463.

[9] P. J. Chung, "DOA estimation methods and algorithms," in *Academic Press Library in Signal Processing*, vol. 3. Amsterdam, The Netherlands: Elsevier, 1994, pp. 599–650.

[10] J. Capon, "High resolution frequency-wavenumber spectrum analysis," *Proc. IEEE*, vol. 57, no. 8, pp. 1408–1418, Aug. 1969.

[11] C. Vaidyanathan and K. M. Buckley, "Performance analysis of the MVDR spatial spectrum estimator," *IEEE Trans. Signal Process.*, vol. 43, no. 6, pp. 1427–1437, Jun. 1995.

[12] J. Li, D. Zheng, and P. Stoica, "Angle and waveform estimation via RELAX," *IEEE Trans. Aerosp. Electron. Syst.*, vol. 33, no. 3, pp. 1077–1087, Jul. 1997.

[13] E. Aboutanios, A. Hassanien, M. G. Amin, and A. M. Zoubir, "Fast iterative interpolated beamforming for accurate single-snapshot DOA estimation," *IEEE Geosci. Remote Sens. Lett.*, vol. 14, no. 4, pp. 574–578, Apr. 2017.

[14] R. O. Schmidt, "Multiple emitter location and signal parameter estimation," *IEEE Trans. Antennas Propag.*, vol. AP-34, no. 3, pp. 276–280, Mar. 1986.

[15] R. Roy and T. Kailath, "Esprit-estimation of signal parameters via rotational invariance techniques," *IEEE Trans. Acoust., Speech, Signal Process.*, vol. 37, no. 7, pp. 984–995, Jul. 1989.

[16] P. Stoica and K. C. Sharman, "Maximum likelihood methods for direction-of-arrival estimation," *IEEE Trans. Acoust., Speech, Signal Process.*, vol. 38, no. 7, pp. 1132–1143, Jul. 1990.

[17] M. Viberg, B. Ottersten, and T. Kailath, "Detection and estimation in sensor arrays using weighted subspace fitting," *IEEE Trans. Signal Process.*, vol. 39, no. 11, pp. 2436–2449, Nov. 1991.

[18] T.-J. Shan, M. Wax, and T. Kailath, "On spatial smoothing for direction-of-arrival estimation of coherent signals," *IEEE Trans. Acoust., Speech, Signal Process.*, vol. ASSP-33, no. 4, pp. 806–811, Apr. 1985.

[19] S. U. Pillai and B. H. Kwon, "Forward/backward spatial smoothing techniques for coherent signal identification," *IEEE Trans. Acoust., Speech Signal Process.*, vol. 37, no. 1, pp. 8–15, Jan. 1989.

[20] W. Du and R. L. Kirlin, "Improved spatial smoothing techniques for DOA estimation of coherent signals," *IEEE Trans. Signal Process.*, vol. 39, no. 5, pp. 1208–1210, May 1991.

[21] F.-M. Han and X.-D. Zhang, "An ESPRIT-like algorithm for coherent DOA estimation," *IEEE Antennas Wireless Propag. Lett.*, vol. 4, no. 12, pp. 443–446, Dec. 2005.

[22] M. Wax and T. Kailath, "Detection of signals by information theoretic criteria," *IEEE Trans. Acoust., Speech, Signal Process.*, vol. ASSP-33, no. 2, pp. 387–392, Apr. 1985.

[23] K. Han and A. Nehorai, "Improved source number detection and direction estimation with nested arrays and ULAs using jackknifing," *IEEE Trans. Signal Process.*, vol. 61, no. 23, pp. 6118–6128, Nov. 2013.

[24] C. Qian, L. Huang, W. J. Zeng, and H. C. So, "Direction-of-arrival estimation for coherent signals without knowledge of source number," *IEEE Sensors J.*, vol. 14, no. 9, pp. 3267–3273, Sep. 2014.

[25] Y. Zhang and B. P. Ng, "MUSIC-like DOA estimation without estimating the number of sources," *IEEE Trans. Signal Process.*, vol. 58, no. 3, pp. 1668–1676, Mar. 2010.

[26] M. Braun, "OFDM radar algorithms in mobile communication networks," Phd dissertation, Inst. Commun. Eng., Karlsruhe Inst. Technol., Karlsruhe, Germany, 2014.

[27] *AWR1642BOOST Single-Chip mmWave Sensing Solution*. [Online]. Available: http://www.ti.com/lit/ug/swru508b/swru508b.pdf

[28] J. Li and P. Stoica, "MIMO radar with colocated antennas," *IEEE Signal Process. Mag.*, vol. 24, no. 5, pp. 106–114, Sep. 2007.

[29] J. Fink and F. K. Jondral, "Comparison of OFDM radar and chirp sequence radar," in *Proc. 16th Int. Radar Symp.*, vol. 1, Jun. 2015, pp. 315–320.

[30] H. Ling and D. W. Jacobs, "Shape classification using the inner-distance," *IEEE Trans. Pattern Anal. Mach. Intell.*, vol. 29, no. 2, pp. 286–299, Feb. 2007.

[31] H. Hung and M. Kaveh, "Focussing matrices for coherent signal-subspace processing," *IEEE Trans. Acoust., Speech Signal Process.*, vol. ASSP-36, no. 8, pp. 1272–1281, Aug. 1988.

[32] *Criterion for Target Number Discrimination*. [Online]. Available: https://bit.ly/2Kuq7Ol

[33] G. P. Kulemin, E. A. Goroshko, and E. V. Tarnavsky, "Land backscattering model for millimeter wave radar," in *Proc. Int. Conf. Modern Problems Radio Eng., Telecommun. Comput. Sci.*, Lviv-Slavsko, Ukraine, 2004, pp. 138–141.

[34] *Short-range Radar Reference Design Using AWR1642*. [Online]. Available: http://www.ti.com/lit/ug/tidud36b/tidud36b.pdf

[35] B. Magaz, A. Belouchrani, and M. Hamadouche, "Automatic threshold selection in OS-CFAR radar detection using information theoretic criteria," *Prog. Electromagn. Res. B*, vol. 30, pp. 157–175, Jan. 2011.

[36] Y. L. Sit and T. Zwick, "Automotive MIMO OFDM radar: Subcarrier allocation techniques for multiple-user access and DOA estimation," in *Proc. 11th Eur. Radar Conf.*, Rome, Italy, Oct. 2014, pp. 153–156.

[37] D. Ivković, M. Andrić, and B. Zrnić, "False alarm analysis of the CATM-CFAR in presence of clutter edge," *Radioengineering*, vol. 23, no. 1, pp. 66–72, Apr. 2014.

TA-SUNG LEE (S'88–M'89–SM'05–F'16) received the B.S. degree from National Taiwan University, in 1983, the M.S. degree from the University of Wisconsin, Madison, WI, USA, in 1987, and the Ph.D. degree from Purdue University, West Lafayette, IN, USA, in 1989, all in electrical engineering. In 1990, he joined the Faculty of National Chiao Tung University (NCTU), Hsinchu, Taiwan, where he holds a position as a Professor with the Department of Electrical and Computer Engineering. From 2005 to 2007, he was the Chairman of the Department of Communication Engineering. From 2007 to 2008 and 2012 to 2013, he was the Vice President for Student Affairs of NCTU. He was the Vice Chairman and Chairman of the IEEE Communications Society Taipei Chapter, from 2005 to 2008, a Board Member of the IEEE Taipei Section, from 2007 to 2010, an Associate Editor of the IEEE Transactions on Signal Processing, from 2009 to 2013, and the IEEE Signal Processing Society Regional Director-at-Large for Region 10, from 2011 to 2013. From 2008 to 2010, he was the Commissioner of the National Communications Commission (NCC), a regulatory agency of Taiwan similar to the FCC, and is responsible for the strategic planning, policy making, and technical regulation for the telecommunications and broadcasting services. From 2013 to 2016, he was the Chairman of the Telecom Technology Center, a government-funded agency for telecommunications Research and Development. He has been the Vice President for Research and Development of NCTU, since 2016, and the Director of the IoT and Intelligent Systems Research Center, since 2017. He is actively involved in research and development in signal processing and system design for wireless communications. He is an IET Fellow. He has received several awards for his research, engineering, and education contributions, including the Young Electrical Engineer Award of the Chinese Institute of Electrical Engineering (CIEE), the Distinguished Electrical Engineering Professor Award of CIEE, the NCTU Distinguished Scholar Award, and the NCTU Teaching Award.

YUN-HAN PAN received the B.S. degree in communication engineering from National Taipei University, New Taipei, Taiwan, in 2017. He is currently pursuing the M.S. degree with the Institute of Communications Engineering, National Chiao Tung University, Hsinchu, Taiwan.
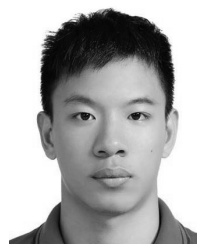
YU-CHIEN LIN received the B.S. degree in engineering and system science from National Tsing Hua University, Hsinchu, Taiwan, in 2016, and the M.S. degree from the Institute of Communications Engineering, National Chiao Tung University, Hsinchu, in 2018, where he is currently a Research Assistant.

KUAN-HEN LIN received the B.S. degree in electrical engineering from the National Taiwan University of Science and Technology, Taipei, Taiwan, in 2016, and the M.S. degree from the Institute of Communications Engineering, National Chiao Tung University, Hsinchu, Taiwan, in 2019.

• • •